Parameters controlling the eruption frequency of long-lived felsic magmatic systems: an example from the Milos volcanic field (Greece).

Xiaolong Zhou[1], Klaudia F. Kuiper[2], Jan R. Wijbrans[3], and Pieter Vroon[2]

[1]Vrije Universiteit Amsterdam
[2]Vrije Universiteit
[3]VU University Amsterdam

November 26, 2022

Abstract

The observation that individual volcanic centres have their own eruption frequencies has been known for a long time but is as yet poorly understood. The key to a better understanding of the mechanisms controlling the eruption frequency comes from integrating accurate geochronology and geochemical data with numerical models. In many silicic volcanic systems, the eruption frequency is studied for short timescales of <1 Ma. Here, we combine two published numerical models to improve our understanding of the eruption frequency in a long-lived (>3 Ma) felsic magmatic system, the Milos volcanic field. From these two models, we interpret the time intervals between magma pulses into the subvolcanic reservoir (t_i), the rates of magma supply (Q_{av}) and chamber growth rates (G_{mc}) as the key parameters controlling the eruption frequency. During the time intervals of 1.5-1.04 Ma and 0.97-0.63 Ma the t_i is longer than 500 years and the volcanic quiescence periods are longer than 350 ka. Furthermore, these periods are characterized by low values for Q_{av} ([?] 0.001 $km^3 \cdot yr^{-1}$) and for G_{mc} (<0.0008 $km^3 \cdot yr^{-1}$). In contrast, during the time intervals of 3.3-1.5 Ma and 0.60-0.06 Ma, the t_i is shorter (<0.5 ka) and the values for Q_{av} (> 0.001 $km^3 \cdot yr^{-1}$) and for G_{mc} (> 0.001 $km^3 \cdot yr^{-1}$) are higher corresponding to frequent eruptions. The parameters t_i, Q_{av}, and G_{mc} appear to determine the eruption frequency of a volcanic system. Changes in one or more of these three parameters of the Milos volcanic field correlate with changes in the tectonic stress field.

Parameters controlling the eruption frequency of long-lived felsic magmatic systems: an example from the Milos volcanic field (Greece).

Xiaolong Zhou[1], Klaudia Kuiper[1], Jan Wijbrans[1], Pieter Vroon[1]

[1]Department of Earth Sciences, VU University Amsterdam, De Boelelaan 1085, 1081 HV Amsterdam, The Netherlands.

Corresponding author: Xiaolong Zhou (z.x.l.zhou@vu.nl)

Key Points:

- A combination of Monte Carlo simulation and thermo-mechanical modelling is applied to the Milos felsic volcanic field
- Modelling suggests that the lithospheric stress field controls the magma supply and magma chamber growth rates of the Milos volcano and therefore also the eruption frequency

Abstract

The observation that individual volcanic centres have their own eruption frequencies has been known for a long time but is as yet poorly understood. The key to a better understanding of the mechanisms controlling the eruption frequency comes from integrating accurate geochronology and geochemical data with numerical models. In many silicic volcanic systems, the eruption frequency is studied for short timescales of <1 Ma. Here, we combine two published numerical models to improve our understanding of the eruption frequency in a long-lived (>3 Ma) felsic magmatic system, the Milos volcanic field. From these two models, we interpret the time intervals between magma pulses into the subvolcanic reservoir (t_i), the rates of magma supply (Q_{av}) and chamber growth rates (G_{mc}) as the key parameters controlling the eruption frequency. During the time intervals of 1.5-1.04 Ma and 0.97-0.63 Ma the t_i is longer than 500 years and the volcanic quiescence periods are longer than 350 ka. Furthermore, these periods are characterized by low values for Q_{av} ($\leq$ 0.001 $km^3 \cdot yr^{-1}$) and for G_{mc} (<0.0008 $km^3 \cdot yr^{-1}$). In contrast, during the time intervals of 3.3-1.5 Ma and 0.60-0.06 Ma, the t_i is shorter (<0.5 ka) and the values for Q_{av} (> 0.001 $km^3 \cdot yr^{-1}$) and for G_{mc} (> 0.001 $km^3 \cdot yr^{-1}$) are higher corresponding to frequent eruptions. The parameters t_i, Q_{av}, and G_{mc} appear to determine the eruption frequency of a volcanic system. Changes in one or more of these three parameters of the Milos volcanic field correlate with changes in the tectonic stress field.

1 Introduction

Despite its importance for the prediction and mitigation of volcanic hazards, there is no clear explanation of the processes responsible for the frequency of volcanic eruptions (e.g. Forni et al., 2018). Voight et al. (1999) showed that small and frequent eruptions with a timescale of hours to years are controlled by the conduit system whereas larger explosive eruptions are controlled by the size of the magma chamber (e.g. Jellinek and DePaolo, 2003). Hildreth and Lanphere (1994) suggested that large strato-cone systems stay active for approximately 500,000 years. Wijbrans et al. (2007) demonstrated that the life cycle of a monogenetic volcanic field can be as long as 3 Ma with a characteristic periodicity in individual eruptions. Several models (e.g. Caricchi et al., 2014; Degruyter and Huber, 2014) for the eruption frequency of magmatic systems mainly focus on large (caldera-forming magnitude) and relatively short timescale (<1.0 Ma) volcanic systems, such as Santorini (e.g. Degruyter et al., 2016), Mt Adams (e.g. Townsend et al., 2019), Laguna del Maule (e.g. Le Mével et al., 2016) and Campi Flegrei (e.g. Forni et al., 2018). The magma supply (e.g. the volume of magma added to a magma chamber), the mechanical properties of the crust (e.g. viscosity and cooling timescale) and the tectonic regime (e.g. extension and compression) are key parameters controlling the eruption frequency, is can be inferred from numerical models for short-lived volcanic centres (e.g. Jellinek and DePaolo, 2003; Degruyter and Huber, 2014; Caricchi et al., 2014 and Townsend et al., 2019). So far, it has been difficult to test such models against natural examples with longer lifetimes as accurate and abundant chronostratigraphic data that can be directly linked to the volcanological and geochemical properties of the erupted products often is lacking.

Here we focus on the Milos Volcanic Field (MVF), a felsic center in the South Aegean Volcanic Arc (SAVA) that has been active for the last 3.3 Ma (e.g. Zhou et al., 2020). This relatively long history of the MVF makes it an excellent natural laboratory to study the eruption frequencies of long-lived felsic systems without large caldera-forming eruptions. We try to explain: (1) temporal changes in the eruption frequency of the MVF; (2) what factors control the eruption frequency, and (3) why periods of volcanic activity alternate with longer periods of volcanic quiescence. We base our study on eruption ages and major element data for most of the major volcanic units of Milos island published by Fytikas et al. (1986), Stewart et al. (2006) and Zhou et al. (2020). We integrate these data to validate two numerical models to better understand the variations in magma supply in terms of flux, injection frequency, and magma chamber growth rate and we correlate these parameters with changes in the regional tectonic stress field during the late Neogene.

2 Geological Background

Milos is a volcanic island in the western part of the SAVA, an arc that is located in the eastern Mediterranean as a result of subduction of oceanic crust belonging to the African plate beneath the Aegean microplate (e.g. Nicholls, 1971; Rontogianni et al., 2011). The westward motion of Anatolia in the northern Aegean in combination with the rollback of the African plate resulted in a mainly extension controlled setting with clockwise and counter clockwise rotation of blocks east and west of the Mid-Cycladic Lineament (Fig.1a; e.g. Walcott and White, 1998, Papazachos, 2019).

The Pliocene andesite-dacite volcanism of the western SAVA volcanic fields (VF), Sousaki, Aegina-Poros-Methana, and Milos are all located in basins that are predominantly associated with N-S and/or E-W trending faults (e.g. Saronikos gulf and Matoon basin, Fig.1a; e.g. Pe-Piper and Piper, 2005b, 2007, 2013). During the early-mid Pleistocene, the E-W faults continued to be active in the Methana volcanic field. However, NE-SW trending strike-slip faults that controlled the formation of the basaltic-rhyolitic lava and voluminous pyroclastics of the Santorini and Milos VF developed in the eastern and central parts of the SAVA (e.g. Pe-Piper and Piper, 2005a; Pe-Piper et al., 2005b). In the mid-late Pleistocene, motion along N or NNW trending normal faults occurs widespread in the western part and ENE-trending motion in the eastern part of SAVA. These normal faults are the result of regional extension that is visible near the island of Santorini as rapid basin subsidence (e.g. Druitt et al., 1999) and on the island of Milos as horst - graben structures (Figure 1b, Papanikolaou et al., 1993).

The MVF volcanic units are exposed on the islands of the Milos archipelago: Milos, Antimilos, Kimolos, and Polyegos. Our study focussed on the largest island of this archipelago, Milos. The MVF is underlain by metamorphic basement rocks on which Neogene fossiliferous marine sediments were deposited (e.g. Van Hinsbergen et al., 2004). During the last 3.3 Ma at least 20 discrete submarine and subaerial eruptions and intrusions constructed the MVF (e.g. Fytikas et al., 1986). The geology, geochronology, and geochemistry of the MVF volcanic units have been described in previous studies (e.g. Fytikas et al., 1986; Stewart and McPhie, 2006; and most recently Zhou et al., 2020). The volcanic history of the MVF can be divided into three periods, each of which is characterized by differences in eruptive flux (Fig. 2; Zhou et al., 2020):

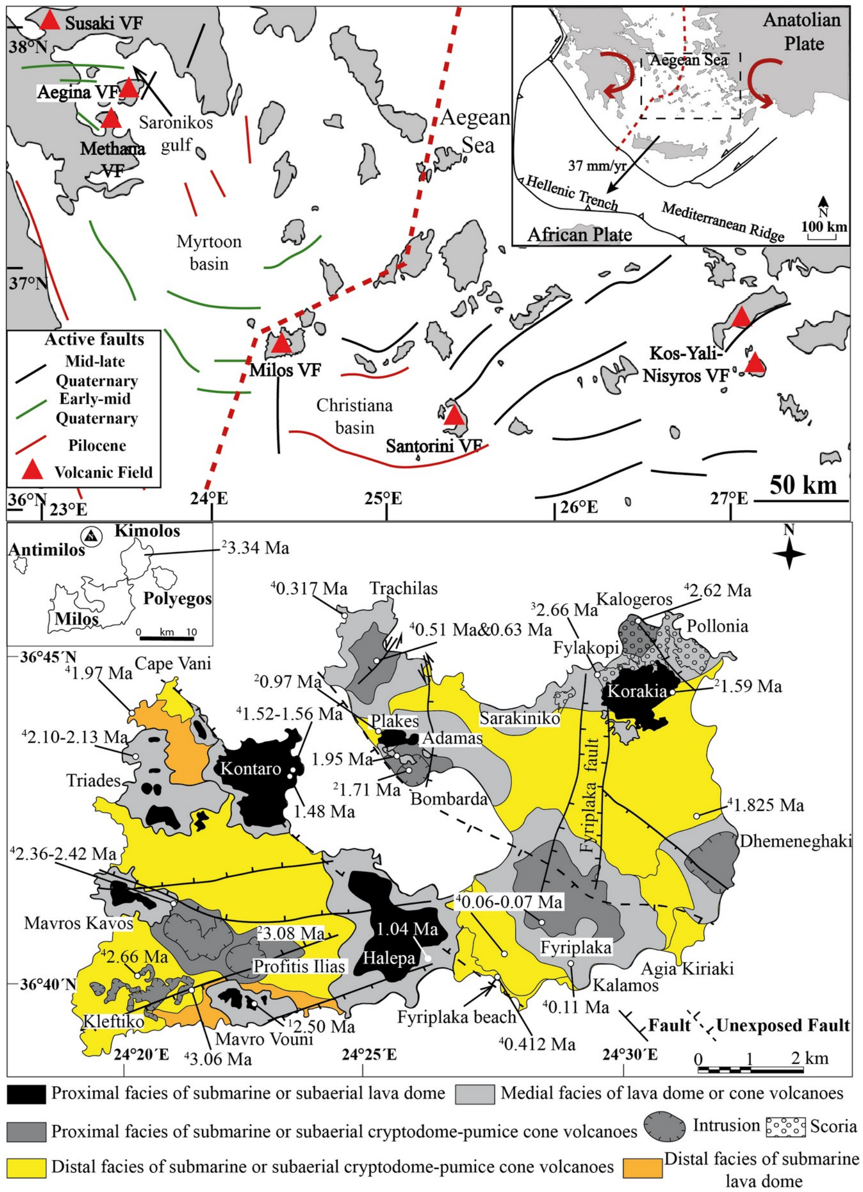

Figure 1. (a) Map of the South Aegean Volcanic Arc (SAVA) with major faults and active volcanic fields (VF). Black arrow represents the GPS-determined plate velocity from Doglioni et al. (2002). The Mid-Cycladic lineament (red-dashed line) separates the clockwise (west) and counter-clockwise (east) paleomagnetic rotations (two red arrows), based on Pe-Piper and Piper (2005a, 2013) and Papazachos (2019). (b) Simplified geological map of Milos with ages of key volcanic centres (after Zhou et al., 2020). Ages are from: 1= Angelier et al. (1977), 2=Fytikas et al. (1986), 3=Stewart and McPhie (2006), 4=Zhou et al., (2020). The descriptions of different proximal, medial and distal volcanic facies of Milos are according to Stewart and McPhie (2006).

(1) Period I (~3.34-2.13 Ma) has a relatively low long term volumetric volcanic output rate (Qe=0.4-1.4×10-5 $km^3 \cdot yr^{-1}$). The volcanic output is mainly from the Profitis Illias and Filakopi felsic cryptodome-pumice cone volcanoes in the SW and NE of Milos, respectively. These two volcanoes produced dacitic-rhyolitic pumice breccia in a submarine environment. The

Mavros Kavos and Mavro Vouni andesitic and dacitic lava domes are from the SW of Milos, which were also formed in the submarine environment. These two domes only contribute minor volcanic units in volume to the MVF. The volume of basaltic-andesitic to dacitic intrusions during this period was limited.

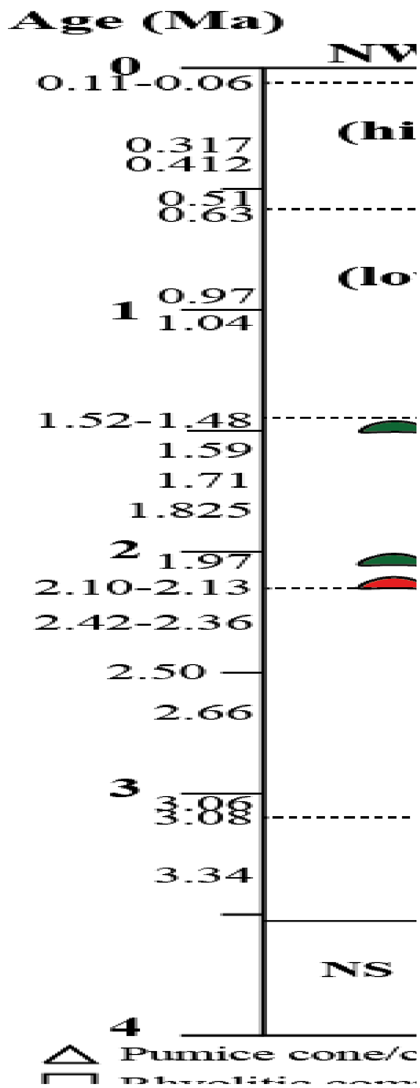

Figure 2. Three periods of different flux of Milos with published age data (modified from Zhou et al., 2020). The left panel represents the major volcanic units of Milos, separated into 4 areas of Milos (NW, NE, SE and SW). Symbol colours: blue=basaltic-andesite or andesite, green=dacite, red=rhyolite. Other abbreviations: NS=Neogene sediments; MB=Metamorphic basement. The start of volcanism (3.34-3.54 Ma) on Milos and the age of the basement underneath Kimolos are not well constrained and indicated with question mark. Other islands in the middle panel represent the islands of Polyegos and Antimilos The Period III of low and high frequency is based on changes in the eruption frequency (details in section 4.2).

(2) Period II (2.13-1.48 Ma) is characterised by a relatively high Qe (0.4-1.4×10-5 $km^3 \cdot yr^{-1}$). The lava dome, Triades, and felsic cone volcanoes, Bombarda and Dhemenghaki, contributed substantial amounts of volcanic products to the MVF in volume of DRE (Dense rock equivalent volumes). They were formed in the submarine environment. Their volcanic products

are dacitic-rhyolitic in composition and widely deposited on the north-western, northern and eastern parts of Milos. Two submarine-to-subaerial andesitic-dacitic lava domes, Kantaro and Korakia, only produced in volume minor amounts of volcanic that were mainly products deposited in the northwest and northeast of Milos, respectively.

(3) Period III (1.48-0.06 Ma) has the smallest Qe (0.2-0.3×10-5 $km^3 \cdot yr^{-1}$) compared with the earlier periods of the Milos volcanic history. The volcanic centres, that contributed limited volumetric products, are described as subaerial dacitic-rhyolitic volcanoes (Halepa and Plakes) and rhyolitic tuff cones (Trachilas and Fyriplaka complexes in the northern and southern parts of Milos) are concentrated along the horst - graben structure found on Milos island.

3 Methods

3.1 Numerical models applied for eruption frequencies

In the last 20 years, three types of models that attempt to link the eruption size, eruption frequency, and magma chamber growth have been published. The first model (Jellinek and DePaolo 2003), the JDP03 model, tries to explain how large volumes of magma can accumulate in the upper crust over time intervals in the range of 10^5-10^6 years. According to JDP03 model, the viscoelastic behaviour of a magma chamber wall prevents over-pressurisation of the magma and therefore eruption. As a consequence, the timescale for chamber pressurisation in the elastic regime is dependent on the size of the magma chamber. The recurrence interval between eruptions in JDP03 model is also correlated with the magma chamber volume, e.g. small magma chambers result in many small eruptions (<100 km^3) whereas large magma chambers result in a few large eruptions (≥100 km^3). Jellinek and DePaolo (2003) suggest that the long-term average flux of magma from depth (=Q_{av}) and magma chamber volume are the main parameters that determine the eruption frequency. De Saint Blanquat et al. (2011), using a similar model, observed a positive correlation between the volume of a pluton and duration of pluton construction, which they attributed to the magma intrusion rate (=Q_{av}).

Caricchi et al. (2014, hereafter referred to as C14) developed a numerical model that uses Monte Carlo simulations to test which variables control the recurrence rate of eruptions with different magnitudes. The C14 model randomly varies the following input parameters: 1.) the long-term average magma supply rate (Q_{av}), 2.) the magma flux during a single injection (Q_{inst}), 3.) the viscosity of the crust (η), the overpressure for an eruption (ΔPcrit), the diameter of the single magma pulses (d) and 4.) the aspect ratio of these single pulses (d/h). The C14 model predicts that large eruptions (>50 km^3) that occur after more than ~0.2 Ma of quiescence are controlled by buoyancy and that smaller, more frequent eruptions (<10 km^3) are controlled by overpressure in a magma chamber. The C14 model results compare well with 24 historical caldera-forming eruptions with caldera diameters of 1-100 km. The outcome of their simulations suggests that Q_{av} determines the volume of a single eruption and, t_i, the time interval between magma injections into the subvolcanic reservoir determines the duration of the magmatic activity, identifying t_i as important for understanding the eruption frequency of a volcanic system.

The third model was originally developed by Degruyter and Huber (2014). This model was further refined in subsequent papers by Townsend et al. (2019) and Huber et al. (2019). We will refer to this group of models as the DHT14&19 model. DHT14&19 model is a numerical thermomechanical model that incorporates the volatile exsolution as an important parameter for the pressurisation of magma chambers. Degruyter and Huber (2014) provided expressions for timescales of magma injection, cooling, and viscous relaxation of the surrounding crust in their equations 33-35 and eruption frequency in their equations 43-45. A thermomechanical algorithm developed in DHT14&19 model shows how the eruption frequency is controlled by different trigger mechanisms (second boiling, magma injection, and buoyancy). It also describes the relations between magma chamber growth rate (G_{mc}), Q_{av}, magma compressibility, eruption frequency, and eruption size. The results of the DHT14&19 model display a good match to the eruption frequency and chamber growth rates of volcanoes in Chile, Italy, Japan, and Greece.

All three models assume that an eruption starts as a dike propagates from the magma chamber to the surface. Heated magma needs to stay below a certain volume fraction of crystals (<0.5) and reach a critical overpressure to erupt, otherwise it will stall in the crust and form a pluton (e.g. Champallier et al., 2008 and Degruyter and Huber, 2014). This overpressure can be caused by the injection of new magma into the magma chamber, crystallisation-induced exsolution of volatiles, and the influence of buoyancy (e.g. Jellinek and DePaolo, 2003; Fowler and Spera, 2010; Malfait et al., 2014; Caricchi et al., 2014). The JDP03 and DHT14&19 models are based on a spherical magma chamber with a constant Q_{av} at a specified temperature and initial dissolved water content (commonly set at ~5 wt.%). The JDP03 model mainly studies the large silicic magma chambers assuming an eruption volume of >100 km^3, which are much larger than most of those assumed for the MVF (Zhou et al., 2020). Therefore, the JDP03 model was not used in this study. The DHT14&19 model focuses on the magma chamber growth during inter-caldera periods in the range of 10-100s ka, and is therefore suitable for short-term fluctuations in the eruption frequency. The C14 model considers a cylindrical shape of the magma chamber and the formation of sills over time instead of a simple sphere. The Q_{av} and the size of the magma chamber in the C14 model are variable within a general range of thermal conditions in the magma reservoir (Caricchi et al., 2014). These settings make the C14 model appropriate for long-term volcanic activity (>1 Ma) but increase the uncertainties on the scales of interest for the case of the MVF. In addition, the C14 model is designed for understanding global scale volcanism and neglects the effects of magma on the thermal and mechanical properties of the magma chamber and surrounding crust (i.e. collapse of the reservoir roof and rheological properties of magma itself).

Thus, a combination of the C14 and DHT14&19 models enables us to better constrain the changes of Q_{av}, t_i, and the magma chamber growth rate (G_{mc}) over timescales appropriate for the MVF. The C14 and DHT14&19 models both consider overpressure and buoyancy as triggers for eruptions. Note that dikes can also propagate from the magma chamber by other external factors, such as crustal extension (Catalano et al., 2014), roof failure (Gregg et al., 2012) and seismic events (Gottsmann et al., 2009).

3.2 Numerical modeling of the MVF as a long-lived volcanic filed

We selected the C14 model as a starting point to explain the eruption frequency of the MVF. In this model, we can adjust the variables Q_{av}, injection pulse diameter (d), and magma chamber shape. This is important because the MVF experienced three periods of different eruptive flux during its long volcanic history, and each of these periods produced variable eruption volumes with different eruption frequencies (Zhou et al., 2020). For example, at least 10 eruptions occurred during 2.1-1.5 Ma contributing ~40% of the total volume to the MVF, whereas between 1.5 and 0.6 Ma only two eruptions from Halepa and Plakes lava domes added

<2% by volume. Therefore, we expect that the Q_{av} and d may have varied significantly during the volcanic history of the MVF. We changed the d between 0.1 and 10 km compared to 1-100 km in the C14 model. This diameter range is smaller due to the small eruption volumes of Milos (<10 km^3 in DRE) than for the large eruption volumes studied by Caricchi et al. (2014). The Q_{av} of the C14 model varies from 0.00001 to 0.1 $km^3 \cdot yr^{-1}$, comparable to the mass inflow rates of Degruyter and Huber (2014) and Townsend et al. (2019). In addition, the ΔPcrit is set between 10-20 MPa, comparable to the values in the C14 and DHT14&19 models. The viscosity of the crust (η_{crust}) was modelled with 10^{18} - 10^{20} Pa. s to fit the felsic magmatic settings of the MVF (e.g. Jellinek and DePaolo, 2003 and Townsend et al., 2019). The t_i varies from 100 to 2500 yr with a step size of 0.1 yr (Table 1). In this C14 model with modified ranges for the input parameters, one million random and simultaneous runs result in a robust constraint on the values of Q_{av} and t_i for the MVF that allows us to study the thermal evolution of the crust underneath Milos.

Table 1

Parameters used in the C14 and DHT14&19 models

Input variables for the Monte Carlo simulations (C14 model)	**Range of value**
Q_{av}: Average flux of magma from depth ($km^3 \cdot yr^{-1}$)	0.00001-0.1
Q_{inst}: The magma flux during a single injection magma ($km^3 \cdot yr^{-1}$)	0.0001-1
η_{crust}: The viscosity of crust (Pa.s)	10^{18}-10^{20}
D_{magma}: The density of the magma ($kg \cdot m^{-3}$)	2300-2700
D_{crust}: The density of the crust ($kg \cdot m^{-3}$)	2700-2800
ΔP_{crit}: The critical overpressure required for eruption (MPa)	10-20
V_{pl}: The volume of cylindrical pulse (km^3)	0.001-8
d: The diameter of each pulse (km)	0.1-10
d/h: The aspect ratio of a single pulse	100
Maximum possible thickness of accumulated magma (km)	20
t_i: the time interval between magma injection (yr)	100-2500
Input variables for the DHT14&19 model	**Related equation**
$\boldsymbol{\rho}$: the density of magma	
V (V_{res}): the volume of the magma chamber (km^3)	
M_{in}: the rate of magma supplying in mass	
$\boldsymbol{\kappa}$: thermal diffusivity of crust	10^{-6} m^2. s^{-1}
$\boldsymbol{\tau}_{in}$: the time scale of magma injecting into magma chamber	$\boldsymbol{\tau}_{in}=\boldsymbol{\rho}V/M_{in}=V/Q_{av}$
$\boldsymbol{\tau}_{cool}$: the time scale of magma cooling in magma chamber	$\boldsymbol{\tau}_{cool}=R^2/\boldsymbol{\kappa}$
$\boldsymbol{\tau}_{relax}$: the time scale for viscous relaxation of the surrounding crust	~16ka or ~160ka
t_{res}: the time elapsed after a reservoir of material above its solidus temperature starts to accumulate magma	$t_{res}=V_{res}/Q_{av}$

Note. $\boldsymbol{\tau}_{in}$, $\boldsymbol{\tau}_{cool}$ and $\boldsymbol{\tau}_{relax}$ are from DHT14&19 model, their equations 33-35 (Degruyter and Huber, 2014) and the Townsend et al. (2019) equations 1-3 (Townsend et al., 2019); V_{res} and t_{res} are from the C14 model (Caricchi et al., 2014).

Caricchi et al. (2014) defined the duration of a magmatic episode as the time interval between the first injection into a magmatic reservoir and the eruption at the surface (see their Fig. 2). However, it is impossible to obtain the exact timing of the first injection. Therefore, we assume that the time interval between two eruptions as the maximum duration of a magmatic episode, in which the first injection of a new episode immediately intrudes into the magmatic reservoir after the last eruption of the previous episode. The duration of a magmatic episode is calculated by the difference between two adjacent $^{40}Ar/^{39}Ar$ and/or K-Ar ages of Milos. If the eruptions occurred at the same location with overlapping $^{40}Ar/^{39}Ar$ and/or K-Ar ages (taken into account the age uncertainty at 2SD) and with similar geochemical compositions (difference of SiO_2 <5 wt%), we assume these eruptions belong to one eruption event. Examples are the eruption ages of 2.36±0.02 - 2.42±0.04 Ma, 2.10±0.02 - 2.13±0.02 Ma and 1.48±0.04 - 1.52±0.02 Ma in the west of Milos and of 0.011±0.04 - 0.06±0.01 Ma in the south (Fig. 1b and Table 2). The dacite (sample G15M0015 of Zhou et al., 2020, 3.06±0.02 Ma) of the Profitis Illias cryptodome, basaltic andesite (sample G15M0016 of Zhou et al., 2020, 2.66±0.01 Ma) of the dyke of Kleftiko and dacitic columnar joint (sample G15M0006, 2.62±0.04 Ma) of Kalegeros cryptodome are intrusions, found in the southwest and northeast of Milos. Therefore, these emplacement ages were not considered as distinct eruption events in this study. Moreover, the eruption age of 1.95±0.45 Ma from the Adamas lava dome (Fig. 1b; sample G15M0004 of Zhou et al., 2020), was not used to calculate the length of a magmatic episode due to its large analytical uncertainty. The eruption age of 3.34±0.06 Ma from Kimolos (Fytikas et al., 1986) was set as the initial point to calculate the length of the first magmatic episode (0.3=3.34-3.04 Ma) of the MVF in the C14 model. Taking these assumptions into account, there are 17 magmatic episodes (Table 2).

Caricchi et al. (2014) used results from thermal modelling of Annen (2009) to quantify the volume of eruptible magma in the magma chamber, and considered that any parcel of magma with less than 50 vol.% of crystals is eruptible. For the MVF, we used the erupted volumes from Zhou et al. (2020). It is important to note that the erupted volume cannot exceed the eruptible portion of the magma body (e.g. Annen, 2009). Blundy and Annen (2016) show that the volume ratio of eruptible magma to magma forming plutons (VPR) is approximately 0.5 for magma chambers smaller than 100 km^3. White et al. (2006) indicated that a ratio of extrusive (erupted) to intrusive volume is approximately 1:5 for most magmatic systems. Therefore, we assume that the eruptible volume of magma of the MVF equals twice the erupted volume.

In the next step, we use the DHT14&19 model to constrain the G_{mc} for each magmatic episode (20-440 ka). The duration of magma cooling (τ_{cool}), injection (τ_{in}), and viscous relaxation of the surrounding crust (τ_{relax}) are required as input parameters (equations 33-35 in Degruyter and Huber, 2014 or equations 1-3 in Townsend et al., 2019). The ratios of τ_{cool}/τ_{in} (θ_1) and τ_{relax}/τ_{in} (θ_2) are used to constrain the G_{mc} for each magmatic episode. Although geomorphological data and isotopic dating (e.g. cosmogenic 36Cl measurements, Singer et al., 2018) can directly provide estimates of τ_{cool}, τ_{in} and τ_{relax} on shorter timescales of less than 100 ka, these data are not available and cannot easily be reconstructed for the >3 Ma MVF. Therefore, we used the C14 model to obtain estimates for these parameters.

The magma reservoir volume (V_{res}) of the C14 model and the magma chamber volume (V) in DHT14&19 model are the same parameters, so we use Vres of the C14 model as an input parameter in the DHT14&19 model. In the C14 model, Caricchi et al. (2014) defined t_{res} as the elapsed time that a reservoir of solid material stays above the solidus temperature and starts to accumulate melt, which is equal to the V_{res} / Q_{av}. The tres is the approximate equivalent of τ_{in} in the DHT14&19 model. Unfortunately, the related τ_{cool} cannot be obtained from the C14 model but is based on equation 34 of Degruyter and Huber (2014) or equation 2 of Townsend et al (2019): τ_{cool} is equal to the square root of the radius of the magma chamber (=√d/2 in the C14 model) divided by a constant, the thermal diffusivity of the crust (10^{-6} m^2/s, Table 1). We assume two values for τ_{relax} of ~16 and ~160 ka. The ~16 ka is consistent with a magma chamber depth of ~7.5 km, a normal continental geothermal gradient of 30ºC/km and a magma composition of andesite-dacite with SiO_2 of volcanic units <72 wt.% (Table 2). The ~160 ka value for τ_{relax} is for

Table 2

Repose time and eruption volume estimates of Milos volcanic units

Database of SiO_2 wt.% and Age	Sample	Volcanic unit	Petrology	SiO_2 wt. %	Age (Ma)	±1σ	ReTime (ka)	±1σ	DRE (km^3)	±1σ	EV (km^3)	±1σ
Zhou et al. (2020)	G15M0008	Fyriplaka complex	Rhyolite	76.7	0.062	0.003						
	G15M0012		Rhyolite	75.5	0.07	0.01	207	20.4	0.18	0.08	0.36	0.16
	G15M0009		Rhyolite	76	0.11	0.02						
	G15M0007	Trachilas complex	Rhyolite	76.7	0.317	0.004	95	5.66	0.39	0.13	0.78	0.26
	G15M0034		Rhyolite	76.9	0.51	0.02	120	28.28	0.39	0.13	0.78	0.26
	G15M0035		Rhyolite	78.4	0.63	0.02	340	63.25	0.39	0.13	0.78	0.26
	G15M0033	Kalamos lava dome	Rhyolite	76.7	0.412	0.004	98	20.4	0.39	0.13	0.78	0.26
	G15M0013	Halepa lava dome	Rhyodacite	72.9	1.04	0.01	440	22.36	0.9	0.3	1.8	0.6
	G15M0019	Kontaro lava dome	Dacite	64.3	1.48	0.02	110	250.8	0.82	0.6	1.64	1.2
	G15M0020		Dacite	-	1.52	0.01						
	G15M0032B	Dhemeneghaki volcano	Rhyolite	75.6	1.825	0.002	145	10.2	7.13	4.13	14.26	8.26
	G15M0021	Triades lava dome	Trachy-dacite	65	1.97	0.01	130	14.14	2.4	1.1	4.8	2.2
	G15M0023		Dacite	73	2.1	0.01	260	14.14	2.4	1.1	4.8	2.2
	G15M0024		Rhyolite	76.6	2.13	0.01						
	G15M0025	Mavros Kavos lava dome	Dacite	69.6	2.36	0.01	300	41.23	0.96	0.44	1.92	0.88
	G15M0026		Dacite	69.6	2.42	0.04						
Fytikas et al. (1986)	M 27	Plakes lava dome	Dacite	63.7	0.97	0.06	70	60.83	0.96	0.44	1.92	0.88
	M103	Korakia lava dome	Andesite	58.7	1.59	0.25	120	254.95	0.82	0.6	1.64	1.2
	M146	Bombarda volcano	Rhyolite	-	1.71	0.05	115	50.04	7.13	4.13	14.26	8.26
	M164	Profitis Illias volcano	Rhyolite-dacite	-	3.08	0.08	260	100	3.1	1.8	6.2	3.6
	M135	Kimolos volcano	-	-	3.34	0.06	-	-	-	-	-	-
Angelier et al. (1977)	Angelier_5	Mavro Vouni lava dome	Andesite	-	2.5	0.09	160	98.49	0.96	0.44	1.92	0.88
Stewart and McPhie (2006)	MIL365	Fylakopi volcano	Rhyolite-dacite	-	2.66	0.04	400	44.72	2.85	1.65	5.7	3.3

Note. ReTime: Repose time-- the time interval between eruptions, which is equal to maximum duration magmatic episode; DRE: Dense rock equivalent volumes of eruption; EV: Eruptible volumes =DRE/0.5; Data of DRE is from Zhou et al. (2020).

a shallower depth (~5 km) with a more thermal mature crust and a rhyolitic magma composition (>72 wt.%) (Karlstrom et al., 2010; Townsend et al., 2019).

In order to validate the outcomes of both the C14 and DHT14&19 models for estimating the τ_{cool} and τ_{in} for the MVF, we compared the C14 and DHT14&19 models for the Laguna del Maule (LdM), Campi Flegrei (CF), Aso, and Santorini volcanic fields. Townsend et al. (2019) provides the estimates of τ_{cool} and τ_{in} for these volcanic fields. In the C14 model we used the data of the eruption ages and volumes of Smith et al. (2011), Crosweller et al. (2012), Parks et al. (2012), and Singer et al. (2014), which are also used by Townsend et al. (2019). We used the same approach to calculate the duration of magmatic episodes and eruptible volumes of the LdM, CF, Aso, and Santorini volcanic fields as used for the MVF and converted their eruption volumes into DRE (Appendix). The eruptible volumes of the large eruptions of Santorini (Minoan and Cape Riva) are considered to be the same as the erupted volumes (~82 and ~15 km^3 in DRE). The CF Epoch 1 is set as the starting point to calculate the first magmatic episode of CF and hence is not included in the estimates of the C14 model. The magma of both the C14 and DHT14&19 models is set to contain 5 wt.% H_2O.

In addition, the G_{mc} based on the C14 model for the Santorini is calculated to compare the results with those of the DHT14&19 model to test the accuracy of our method by comparing our model results with those of previous studies (e.g. Degruyter et al., 2016; Townsend et al., 2019, 2020). Townsend et al. (2019) estimated the Q_{av} and G_{mc} of Santorini in pre- and post-Minoan periods spanning from Cape Riva (~0.021 Ma) to recent eruptions. We extended the pre-Minoan to the Cape Therma 1 (~0.36 Ma) to include most of the major explosive eruptions. The SiO_2 contents of the Santorini volcanic units are collected from Druitt et al. (1999). The data of DRE volume and the maximum duration for the Santorini volcanic episodes were calculated from Crosweller et al. (2012).

4 Results

4.1 Accuracy of the C14 model for estimates of τ_{cool}, $\tau_{in,}$ and G_{mc}

The output of the C14 model provides constraints on the V_{res} and Q_{av} of the LdM, CF, Aso, and Santorini volcanic fields. The comparison between the estimates of the C14 (t_{res} and τ_{cool_cal}) and the DHT14&19 (τ_{in} and τ_{cool}) models is shown in Figure 3. The error bars of τ_{cool} and τ_{in} are not given because Townsend et al. (2019) did not provide those.

There is a good match between tres and τ_{in} for magmatic systems with short timescales (<10 ka) of magma injection and small eruptions Aso, CF Epoch 2+3, and Santorini post-Minoan (Fig. 3a). In magmatic systems with relatively long timescales (>10 ka) of magma injection and caldera-forming eruptions (Santorini pre-Minoan and LdM EPG), the tres based on the C14 model does not overlap with the τ_{in} of the DHT14&19 model. However, this method is still suitable to estimate τ_{in} for the MVF because the C14 model with modified input parameters (section 3.2) is designed for small eruptions (<10 km^3 in DRE). In Figure 3b, the τ_{cool_cal} of the C14 model is comparable to the τ_{cool} from the DHT14&19 model for both small and large eruptions.

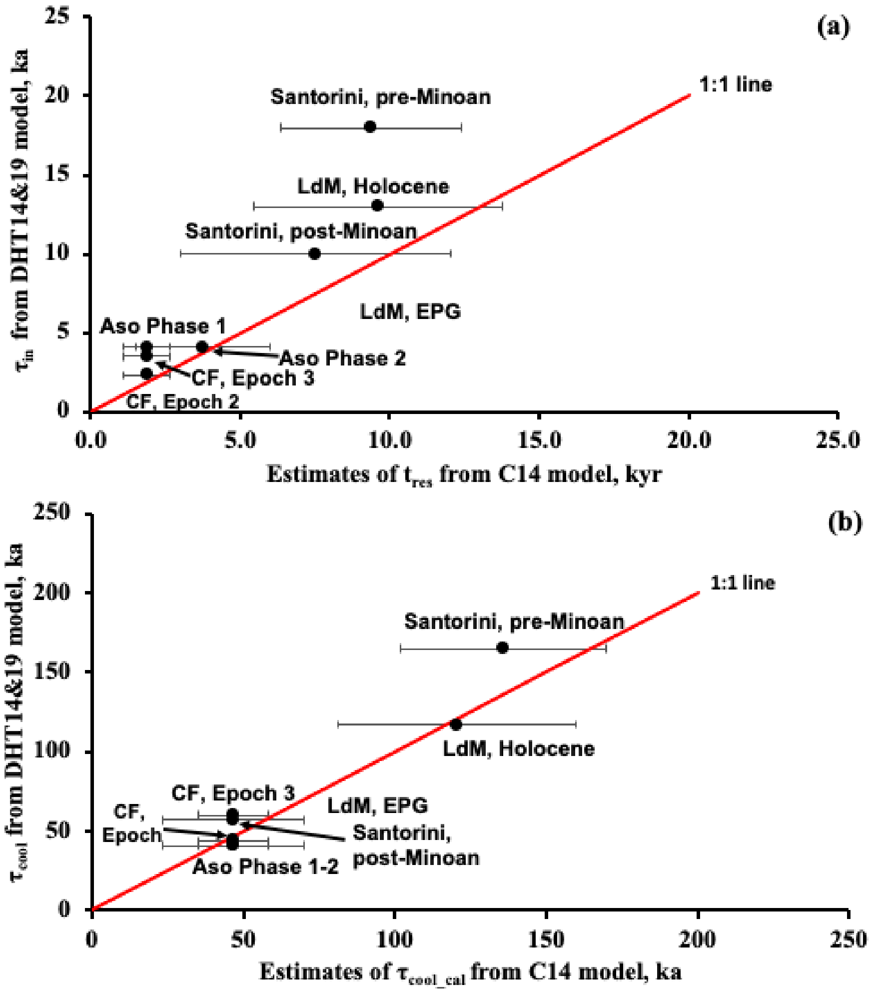

Figure 3. (a) Comparison of the $\mathbf{t_{res}}$ from C14 and the $\boldsymbol{\tau_{in}}$ from the DHT14&19 models. The $\mathbf{t_{res}}$ is equal to the magma chamber volume (the reservoir volume—V_{res} in C14 model) divided by magma supply rate (average flux of magma from depth, Q_{av}). (b) Comparison of τcool_calc and τcool. The τcool is derived from DHT14&19 model, whereas the τcool_calc is equal to the square of the radius of a magma chamber (=d/2 in C14 model) divided by the thermal diffusivity of crust (10-6 m2/s). The τcool and τ_{in} represent the timescales for magma cooling and injection in DHT14&19 model. The error bars of τcool and τ_{in} from the DHT14&19 model are not given since uncertainties were not given by Townsend et al. (2019). Abbreviations: LdM Holocene=Laguna del Maule Holocene; LdM-EPG=Laguna del Maule Early-Post-Glacial period; CF2=Campi Flegrei Epoch 2 and CF3= Campi Flegrei Epoch 3.

4.2 Geological constraints for Milos and Santorini and their implications for the models

The age distribution of the volcanic units of Milos indicates that the eruption frequency varied during its volcanic history (Fig. 2). Based on the variations in whole-rock SiO_2 content and the duration of magmatic episodes, we have further divided the volcanic history of Milos into four periods (Fig. 4a). The first two periods are consistent with the Period I and II of Zhou et al. (2020) which are also referred to as Period I and II in this study. We only further divided the Period III of Zhou et al. (2020) into two periods based on their different eruption frequency (Period III with low and high frequency). The Period I (~3.3 to 2.13 Ma; Zhou et al., 2020) is

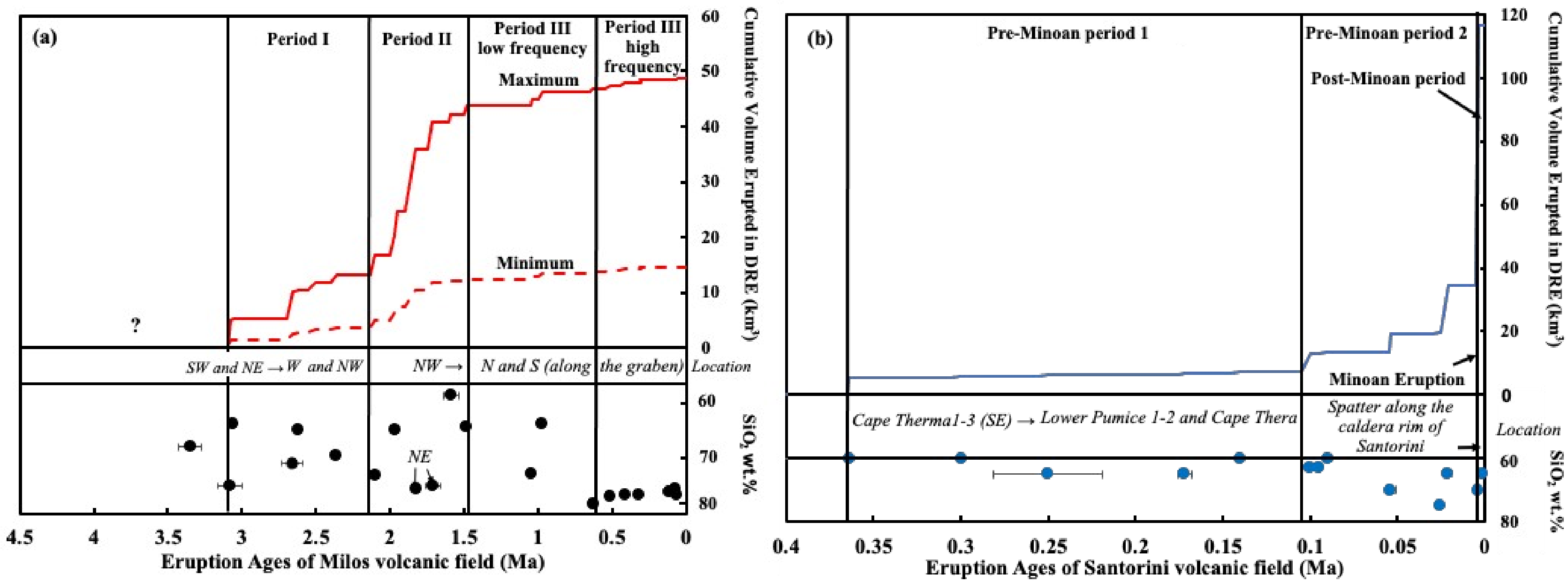

Figure 4. Cumulative eruption volume versus time for the volcanic deposits of (a) Milos and (b) Santorini. The cumulative eruption volume curves of Fig. 3a and 3b were modified based on Zhou et al. (2020) and Crosweller et al. (2012), respectively. Composition (SiO_2 wt.%) of the erupted products are shown (data from Fytikas et al., 1986, Druitt et al., 1999a and Zhou et al., 2020). The exact volume of Milos volcanic products between 3.5 and 3.08 Ma is not well constrained and indicated with a question mark. Note the shift to more felsic compositions over time for both volcanic fields. Only the approximate estimates for Santorini are reported due to the unknown uncertainties. Abbreviations: SW=South West; W=West; NW=North West; N=North; S=South; SE=South East; VF=Volcanic Field.

characterised by magmatic episodes with a long duration of >150 ka and the composition of Period I changes from dacitic to rhyolitic (63-75 wt. % of SiO_2). The Period II (2.13-1.48 Ma; Zhou et al., 2020) has at least five relatively short magmatic episodes (100-150 ka). The composition of Period II units has a relatively wider range compared to that of Period I, varying from andesitic to rhyolitic in composition (57-75 wt. % of SiO_2). The Period II was followed by only two eruptions between 1.48 and 0.60 Ma which we define here as Period III with low frequency. During the Period III with low frequency, the magmatic episodes are very long (>300 ka) and the volcanic units became more felsic. In the last period (0.60-0.06 Ma), defined as Period III with high frequency, the magmatic episodes are mainly shorter than 120 ka and produced pumice with SiO_2 >75 wt.%. There is a risk that not all eruptions of the MVF in the past 3.5 Ma are included and therefore model input data is not complete. All the major volcanic units are included in this study based on the results of previous studies (e.g. Fytikas et al., 1986; Stewart and McPhie, 2006; Zhou et al., 2020).

The pre-Minoan period of Santorini was separated into pre-Minoan periods 1 and 2 based on the composition of volcanic products, eruption frequency, and volume (Fig. 4b). The pre-Minoan period 1 includes the magmatic episodes of Cape Therma 1-3 (0.36-0.25 Ma), Lower Pumice 1-2 (0.18-0.17 Ma) and Cape Thera (~0.14 Ma), which only added ~7.4 km^3 in DRE of andesitic-dacitic and rhyolitic volcanic units (Druitt et al., 1999). The pre-Minoan period 2 added a larger volume (~27 km^3 in DRE) to Santorini than period 1 and the composition of volcanic units became more felsic (andesite—rhyolite) from ~0.1 to 0.021 Ma (Cape Riva). The eruptions of the pre-Minoan period 2 occur along a pre-existing caldera rim. The last caldera-forming eruption of Santorini, the Minoan eruption, contributed ~70% (rhyodacite) by volume (DRE) covering most of Santorini. Since then only ~0.05 km^3 (DRE) of dacitic lavas were produced, mainly on the Kameni islands (Druitt et al., 1999), which are considered to represent the post-Minoan period.

4.3 Results of the DHT14&19 and C14 models for Milos and Santorini VF

Figure 5 shows the results of the C14 model with the input parameters tailored to the Milos and Santorini volcanic fields. Buoyancy-driven eruptions generally have larger eruptible magma volumes in their magma reservoirs (>10 km^3) (Caricchi et al., 2014). Buoyancy did control at least one eruption (eruptible volume >10 km^3 in DRE) during the Period II of the MVF (2.13-1.48 Ma), resulting in a V_{res} of 0-45 km^3, Q_{av} of 0.002-0.003 $km^3.yr^{-1}$ and t_i= 0.1-0.2 ka. Furthermore, the G_{mc} varies between 0.001-0.0001 $km^3 \cdot yr^{-1}$ based on the DHT14&19 model. The other eruptions of Milos are mainly triggered by magma injection. During the Period I and II of the MVF, the long duration of magmatic episodes (>120 ka) and relatively large eruptible volumes (1-10 km^3 DRE) could be triggered by either buoyancy or magma injection or both (Fig. 5). With relatively infrequent magma injections (t_i= 0.2-0.5 ka), the V_{res} (<30 km^3) and Q_{av} (<0.003 $km^3 \cdot yr^{-1}$) of these two periods are small, but the G_{mc} (0.01-0.001 $km^3 \cdot yr^{-1}$) is high. The Period III with low frequency of the MVF (1.48-0.60 Ma) is characterised by a long t_i (0.5-2.5 ka), low Q_{av} (<0.001 $km^3 \cdot yr^{-1}$), and small V_{res} (<20 km^3). The G_{mc} of this period significantly decreased from more than 0.001 to less than 0.0001 $km^3 \cdot yr^{-1}$. An exception is a short (<100 ka) magmatic episode at 0.97 Ma with G_{mc} between 0.001 and 0.01 $km^3 \cdot yr^{-1}$. Most of the young volcanic eruptions on Milos and Santorini are characterised by short magmatic episodes (<120 ka) and small eruptible volumes (<1 km^3, Fig. 5). The results of the C14 model show a variable V_{res} (5-10 km^3 for the magmatic episode duration ≤5 ka and 30-45 km^3 for >5 ka), high Q_{av}

(0.003-0.005 $km^3 \cdot yr^{-1}$), and frequent magma injection (t_i = 0.1-0.2 ka) for these young volcanic units (Figure 5b and 5c). However, the outcome of the DHT14&19 model shows different G_{mc} for these young units of Milos and Santorini (Fig. 6a-c). During the pre-Minoan period 1-2, the G_{mc} of Santorini mainly varies between 0.001 and 0.003 $km^3 \cdot yr^{-1}$ based on the C14 model, comparable to that of the DHT14&19 model (~0.001 $km^3 \cdot yr^{-1}$). The G_{mc} (>0.001 $km^3 \cdot yr^{-1}$) of the young Milos volcanic units (<0.6 Ma, Fig. 6) is lower than those of the pre-Minoan period 1 and 2 of Santorini but comparable to the estimate of the post-Minoan period from Townsend et al. (2019).

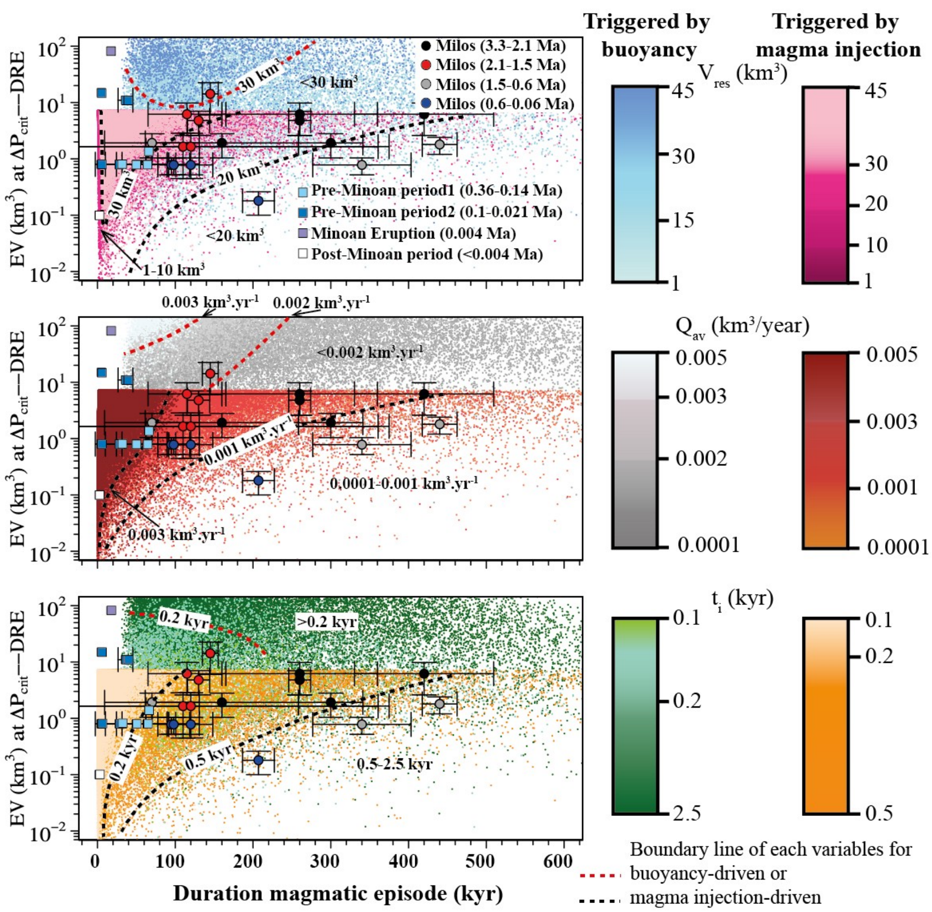

Figure 5. Results of Monte Carlo simulations based on the C14 model (Caricchi et al., 2014) compared to the eruptions of Milos (four periods: 3.3-2.1, 2.1-1.5, 1.5-0.6 and 0.6-0.06 Ma) and Santorini volcanic fields (0.36-0.003 Ma). **(a)** C14 model with a range of 1-45 km^3 magma chamber volumes. This diagram shows that most small eruptible volumes (<10 km^3) of Milos and Santorini are triggered by magma injection, and the large ones (>10 km^3 in DRE) are generated by buoyancy. **(b)** C14 model for different Q_{av}. The Q_{av} varies from 0.0001 to 0.005 $km^3 \cdot yr^{-1}$. **(c)** C14 model with variable time intervals between injections (t_i). The t_i ranges between 100 and 2500 yr with an interval of 0.1 yr. Most small volume eruptions of Milos and Santorini can be explained with Q_{av} =0.001-0.003 $km^3 \cdot yr^{-1}$ and t_i=100-2500 years. The larger eruptions of Milos and Santorini are triggered by buoyancy with a relatively higher Q_{av} (0.002-0.005 $km^3 \cdot yr^{-1}$) with short t_i (100-200 years). Several magmatic episodes of Milos with long duration (>300 ka; grey circle) and small eruptible volume (<1 km^3 in DRE) are fed by a low flux of magma ($Q_{av} \leq$ 0.001 $km^3 \cdot yr^{-1}$) with long t_i (500-2500 years).

In Figure 5a, the buoyancy-triggered Minoan caldera-forming and the large volume Cape Riva eruptions of Santorini cannot be modelled with the C14 model with the modified input parameters (section 3.2) due to their very short magmatic episodes (<5 ka). However, these two exceptions will not affect the discussion of the MVF because they are not relevant for the small-volume eruptions. Furthermore, the estimation on Q_{av} of the post-Minoan period is likely inaccurate due to the very short magmatic episode (~2 ka).

5 Discussion

5.1 The influence of t_i, Q_{av} and G_{mc} on the eruption frequency

Based on the C14 and DHT14&19 models, we can distinguish variations in potential parameters controlling the eruption frequency of the long-lived Milos volcanic field. The potential parameters include the injection frequency ($1/t_i$), the average long-term flux of magma from deep (Q_{av}) and magma chamber growth rate (G_{mc}) (Fig. 7). The Period I, II, III with low and high frequency of the Milos volcanic history have different and systematic variations in t_i, Q_{av}, and G_{mc}:

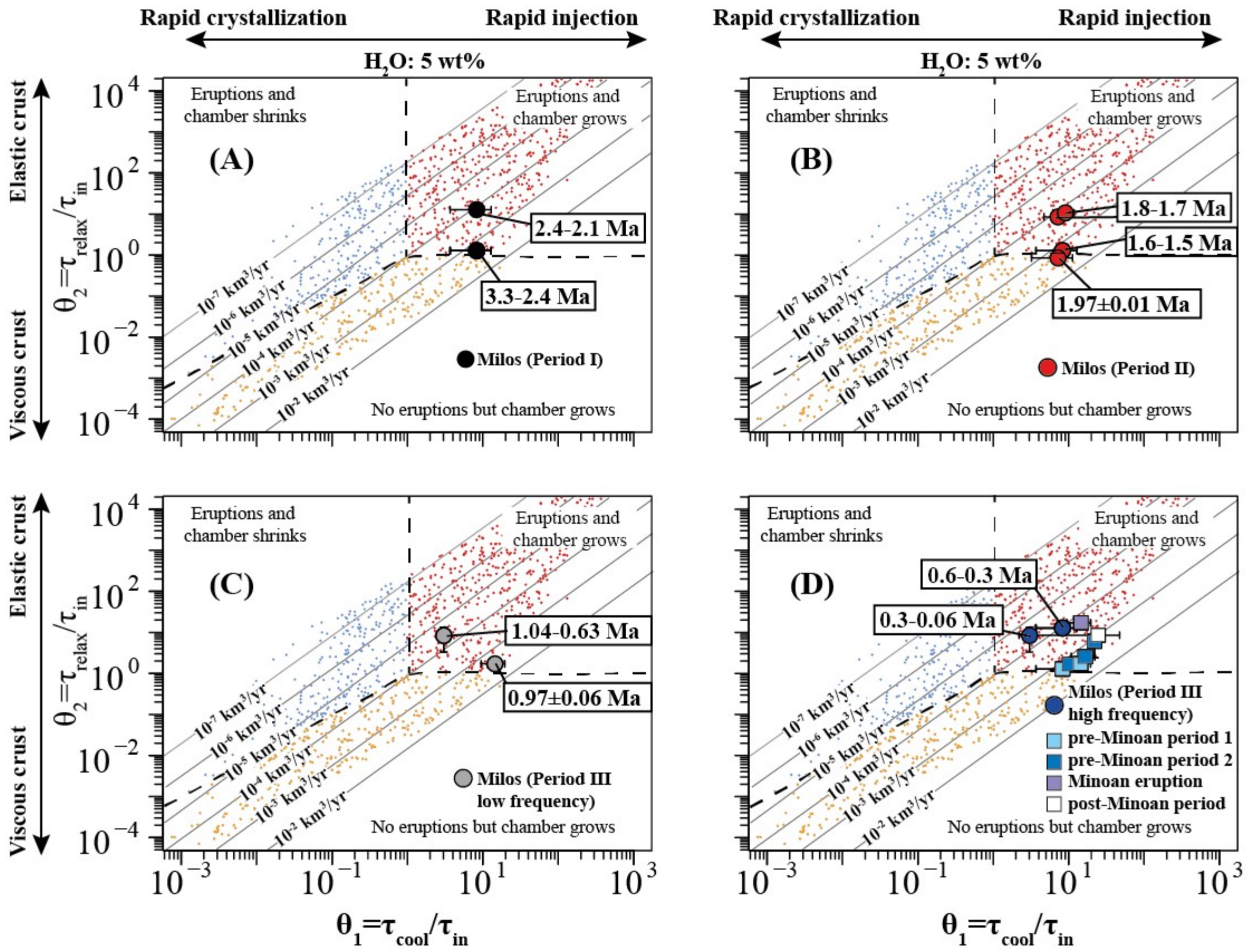

Figure 6. Magma chamber growth rates for Milos (3.3-0.97 Ma) **(A-C),** Milos (0.6-0.06 Ma) and Santorini **(D)** for magmas with 5 wt.% water, based on the thermo-mechanical model of Townsend et al. (2019). The $\boldsymbol{\tau}_{\mathbf{relax}}$ is set as two constants, 16 ka as in Townsend et al. (2019) which is appropriate for a chamber at ~7.5 km depth with a normal geothermal gradient (30 °C/km), and 160 ka corresponding to a shallow depth (~5 km) with more thermal mature crust (Townsend et al., 2019). Data sources for Santorini are obtained from the model results of Figure 4. See Appendix I for details.

During the Period I (~3.3-2.1 Ma) the SiO_2 content of the MVF volcanic products are more variable (andesite-rhyolite) before 2.7 Ma and dacitic after 2.7 Ma (Fig. 4a). The relatively high Q_{av} (>0.001 $km^3.yr^{-1}$) and moderate t_i (0.2-0.5 ka) correspond to a relatively high G_{mc} (>0.001 $km^3 \cdot yr^{-1}$). These characteristics could keep the magma molten and eruptible during the Period I even though the eruption frequency is low (>200 ka). Magmas were probably stored in upper crustal reservoirs where they could fractionate to more felsic compositions and increase the timescale for viscous relaxation of the surrounding crust (τ_{relax}) up to ~160 ka (see section 3.2). The increased τ_{relax} leads to a decrease in G_{mc} (0.0001-0.0003 $km^3 \cdot yr^{-1}$) at the end of the Period I (Fig. 7c).

The Period II (2.13-1.48 Ma) consists of relatively more frequent eruptions (<160 ka) and has similar estimates for Q_{av}, t_i, and G_{mc} as obtained for the first period. However, two magmatic episodes (1.6-1.5 Ma and 1.97 Ma) of the Period II show higher Q_{av} (>0.002 $km^3 \cdot yr^{-1}$), more frequent injection (t_i<0.2 ka) and lower G_{mc} (0.0001-0.0003 $km^3 \cdot yr^{-1}$). These two episodes produced rhyolitic volcanic units in the north-eastern part of Milos. The high viscosity of the surrounding crust could have resulted in a decrease of the G_{mc}.

The Period III with low frequency (1.48 to 0.60 Ma) is characterised by a significantly lower Q_{av} (<0.001 $km^3 \cdot yr^{-1}$), G_{mc} (<0.0001 $km^3 \cdot yr^{-1}$), and long t_i (>0.5 ka), that corresponds to the low eruption frequency (>350 ka at average) during this period. These parameters resulted in a small heat flux from deep (e.g. hot-zone, Annen et al., 2006) that was probably too low to cause fast accumulation of eruptible magma (e.g. Caricchi et al., 2014). Therefore, during a ~1 Ma period with low eruption frequency the magma chamber grew slowly (Fig. 6c) and plutons probably formed in the crust underneath Milos.

During the Period III with high frequency (0.60 Ma-present), there are sudden increases in Q_{av} (>0.001 $km^3 \cdot yr^{-1}$) and injection frequency ($1/t_i$ >2 ka^{-1}). These abrupt changes resulted in several small-volume eruptions (eruptible volume <1 km^3) until 0.3 Ma. Between 0.30-0.06 Ma, the Q_{av} and t_i have similar characteristics to those of the Period III with low frequency after a relatively long period of quiescence (~200 ka). All volcanic units of 0.60-0.06 Ma are composed of rhyolitic pumice and lava. The G_{mc} of this period is not higher than 0.0001 $km^3 \cdot yr^{-1}$ due to the long $\boldsymbol{\tau}_{relax}$, similar to the other magmatic episodes that produced rhyolites. The t_i of 0.6-0.3 Ma of the MVF is comparable to the pre-Minoan period 1-2 (0.36-0.021 Ma) of Santorini, whereas the Q_{av} and G_{mc} are lower than those of the pre-Minoan period 1-2. The relatively mafic eruptible magma of the pre-Minoan period 1-2 and high Q_{av} probably resulted in the very high G_{mc} (>0.002 $km^3 \cdot yr^{-1}$), which could provide conditions for the Minoan caldera-forming eruption.

5.2 Variable t_i, Q_{av} and G_{mc} as indicators for changes in tectonic stress

Three time slots are separating the Milos volcanic history (2.0-1.9 Ma, 1.5-1.4 Ma, and 0.6-0.5 Ma), that overlap with abrupt changes in t_i, Q_{av}, and G_{mc}. An external trigger, such as changes in the regional tectonic stress field (e.g. Jellinek and DePaolo, 2003; Caricchi et al., 2014), could have caused the abrupt changes in these parameters. There were four major changes in the regional stress field (Fig. 7d) during the development of the Milos VF. Van Hinsbergen et al. (2004) found that marine sediments underlying the volcanic units of Milos record up to 900 m of subsidence between 5.0-4.4 Ma, approximately 1.5 Ma before the first volcanic eruptions occurred in the MVF (~3.3 Ma). They interpreted this subsidence as evidence for the start of (regional) extension. Armijo et al. (1992) inferred that the change in direction of the major extensional faults from N-S to E-W in the late Pliocene (~2-4 Ma) resulted from the collision

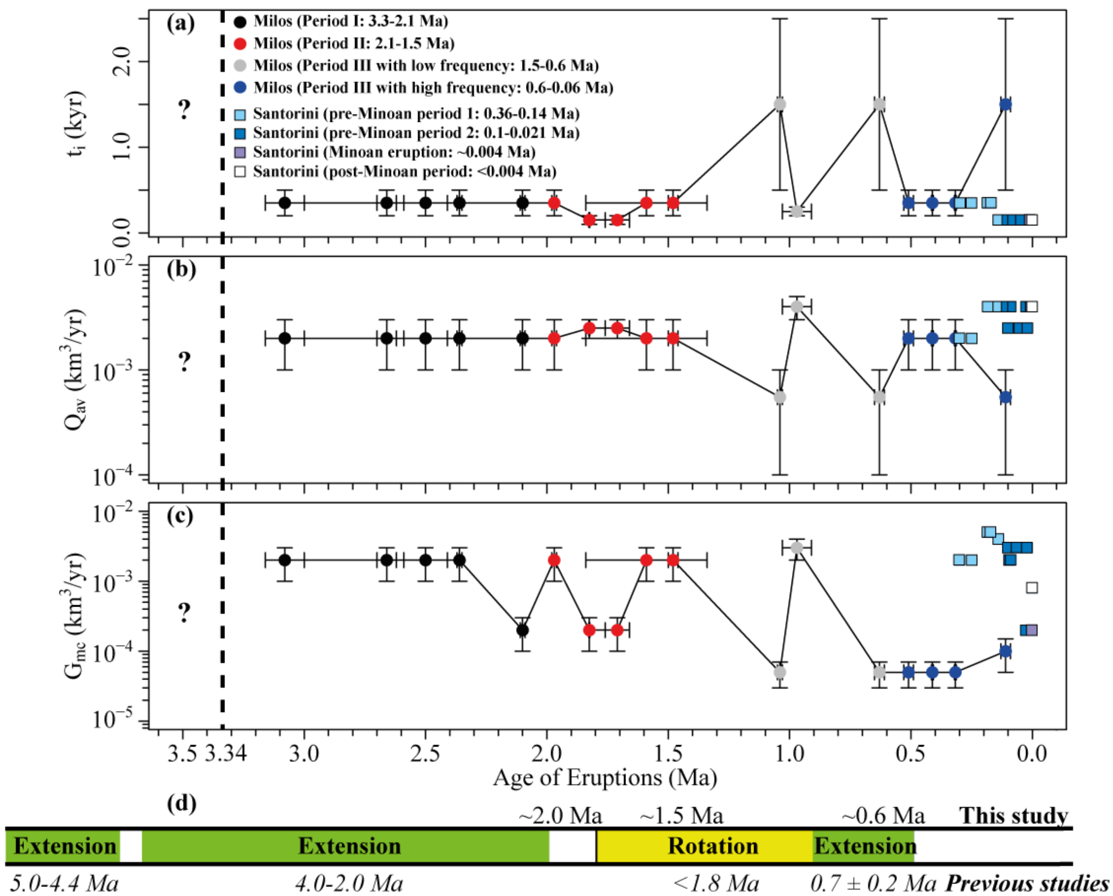

Figure 7. (a) The variation of t_i (time interval between magma injections) versus the eruption age for volcanic units of the Milos and Santorini volcanic fields. (b) The variation of Q_{av} (the average long-term flux of magma from deep) versus eruption ages for volcanic units of Milos and Santorini volcanic fields. (c) The variation of G_{mc} (magma chamber growth rate) versus eruption ages for volcanic units of Milos and Santorini volcanic fields. (d) Tectonic stress field in the SAVA during the last 5 Ma (Armijo et al., 1992; Duermeijer et al., 2000; Piper and Perissoratis, 2003; Van Hinsbergen et al., 2004). The error bars for the data of the Santorini volcanic field are larger than the scale of the figure and are provided in the Appendix. The variables t_i, Q_{av} and G_{mc} of the Milos volcanic field between 3.5 and 3.34 Ma are unknown and indicated with a question mark. During periods of extension the injection frequency ($1/t_i$), Q_{av} and G_{mc} are larger than in the periods of rotation (and compression). See text for further discussions.

between the Aegean plate and the northern margin of Africa. The periods of the tectonic stress transitions overlap with rapid changes in our estimates of Q_{av}, t_i, and G_{mc} at ~2.0 Ma when felsic volcanic units were formed in the MVF (Fig. 7). It is conceivable that during (regional) extension, it became easier for viscous felsic melts to ascend to the surface, which may have resulted in higher magma fluxes, chamber growth rates, and more frequent injections. Duermeijer et al. (2000) suggested that during the Pleistocene (at least younger than ~1.8 Ma) both clockwise and anticlockwise rotations of the old western and young eastern SAVA occurred, respectively. Milos is located on or close to the Mid Cycladic lineament, a zone separating these two rotating blocks (Fig. 1). Therefore, the area of Milos could have experienced a compressional stress field due to rotations of crustal blocks north-west and south-east of the Mid-Cycladic lineament during the Pleistocene. Compression may have suppressed the magma flux and injection frequency of Milos magmatic system since 1.5 Ma (Fig. 7). This in turn may have caused the low G_{mc} between 1.55 and 0.59 Ma, except for the magmatic episode of <100 ka which could have been triggered by a fault activated by rotation (e.g. Jellinek and DePaolo, 2003). Piper and Perissoratis (2003) suggested that the Aegean region experienced a change in the tectonic stress field around 0.7 ± 0.2 Ma when predominantly E-W faults were superseded by N-S faults. During the third extension (0.9-0.5 Ma) the magma flux, frequency of magma injection, and chamber growth rate increased again (Fig. 7). The regional change in the tectonic stress field, compression-extension, could also have been a factor for the caldera-forming eruptions of Santorini. Differences in the local tectonic stress fields may have caused more frequent injections and a higher chamber growth rate at Santorini than at the MVF (Fig. 7).

Pe-Piper and Piper (2013) found a similar change in tectonic stress field for the Methana volcanic field (Fig. 1a). Volcanism on Methana started at ~3 Ma during a phase of regional E-W extension. Extension occurred again around ~2.1 Ma as the NE-SW strike-slip faults began to form that could have resulted in the formation of calderas (e.g. Pe-Piper and Piper, 2013). The last phase of extension on Methana started at ~0.4 Ma when the E-W faults were active near the Methana and Milos volcanic fields. In addition, Elburg et al. (2018) suggested a period of compression for Methana between 3.5 and 1.4 Ma, overlapping with the timing inferred from this study (~1.55 Ma).

6 Conclusions

(1) The ~3.3 Ma volcanic history of Milos can be subdivided into four periods (Period I, II, III with low and high eruption frequency) based on the frequency of eruptions and major element composition of the eruption products. We applied two numerical models, one of Caricchi et al. (2014) (C14) and the other from Degruyter and Huber (2014) and Townsend et al. (2019) (DHT14&19) The C14 model is used to investigate which parameters might be responsible for the alternation of periods with eruptions versus periods of quiescence. The DHT14&19 model provides tools to relate the eruption frequency to the magma chamber growth of the individual magmatic episodes. The results of both models suggest that a high magma flux (Q_{av}>0.001 $km^3 \cdot yr^{-1}$), and frequent injections (t_i<0.5 ka) result in a high rate of magma chamber growth (>0.001 $km^3 \cdot yr^{-1}$) and frequent eruptions on Milos and Santorini. On the other hand, a low Q_{av} (<0.001 $km^3 \cdot yr^{-1}$), infrequent injections (t_i>1.0 ka), and high viscosity of the surrounding crust do not result in fast magma chamber growth and frequent eruptions.

(2) We suggest that a change in tectonic stress field in the SAVA between 2-4 Ma and 0.9-0.5 Ma from compression to extension opened channels in the crust that enabled a higher magma flux and more frequent injections at ~2.1 Ma and ~0.6 Ma. The clockwise and anticlockwise rotations of crustal blocks near Milos between 1.5-~0.6 Ma). co resulted locally in a compressional stress field that inhibited magmas from rising to the surface, resulting in the formation of plutons.

(3) Based on our two models using rock major element chemistry and geochronological data, we propose that the abrupt changes in Q_{av}, t_i, and G_{mc} can best be explained by changes in the tectonic stress field.

Acknowledgments

We acknowledge the Greek Institute of Geology and Mineral Exploration (IGME) for permission to conduct fieldwork on Milos. We would like to thank Meredith Townsend and Luca Caricchi for providing their computer code and extensive instructions on how to use it. XZ would like to acknowledge a China Scholarship Council (CSC) grant (no. 201506400055). The $^{40}Ar/^{39}Ar$ facility of the VU is covered by NWO grant 834.09.004. This research benefitted from funding from the European Research Council under the European Union's Seventh Framework Programme (FP7/2007-2013)/ERC grant agreement no. 319209. All data from the volcanic systems come from published literature, except for the $^{40}Ar/^{39}Ar$ data for the Milos Volcanic Field from Zhou et al. (2020) which is still in press. Please refer to the supporting information for the $^{40}Ar/^{39}Ar$ data, input and output files for all model simulations.

References

Annen, C. (2009). From plutons to magma chambers: Thermal constraints on the accumulation of eruptible silicic magma in the upper crust. Earth and Planetary Science Letters, 284(3–4), 409–416. https://doi.org/10.1016/j.epsl.2009.05.006

Annen, Catherine, Blundy, J. D., & Sparks, R. S. J. (2006). The genesis of intermediate and silicic magmas in deep crustal hot zones. Journal of Petrology, 47(3), 505–539. https://doi.org/10.1093/petrology/egi084

Armijo, R., Lyon-Caen, H., & Papanastassiou, D. (1992). East-west extension and Holocene normal-fault scarps in the Hellenic arc. Geology, 20(6), 491–494.

Blundy, J. D., & Annen, C. J. (2016). Crustal magmatic systems from the perspective of heat transfer. Elements, 12(2), 115–120. https://doi.org/10.2113/gselements.12.2.115

Briqueu, L., Javoy, M., Lancelot, J. R., & Tatsumoto, M. (1986). Isotope geochemistry of recent magmatism in the Aegean arc: Sr, Nd, Hf, and O isotopic ratios in the lavas of Milos and Santorini-geodynamic implications. Earth and Planetary Science Letters, 80(1–2), 41–54. https://doi.org/10.1016/0012-821X(86)90018-X

Caricchi, L., Annen, C., Blundy, J., Simpson, G., & Pinel, V. (2014). Frequency and magnitude of volcanic eruptions controlled by magma injection and buoyancy. Nature Geoscience, 7(2), 126–130. https://doi.org/10.1038/ngeo2041

Caricchi, L., Burlini, L., Ulmer, P., Gerya, T., Vassalli, M., & Papale, P. (2007). Non-Newtonian rheology of crystal-bearing magmas and implications for magma ascent dynamics. Earth and Planetary Science Letters, 264(3–4), 402–419. https://doi.org/10.1016/j.epsl.2007.09.032

Catalano, S., Tortorici, L., & Viccaro, M. (2014). Regional tectonic control on large size explosive eruptions: Insights into the green tuff ignimbrite unit of pantelleria. Journal of Geodynamics, 73, 23–33. https://doi.org/10.1016/j.jog.2013.10.008

Champallier, R., Bystricky, M., & Arbaret, L. (2008). Experimental investigation of magma rheology at 300 MPa: From pure hydrous melt to 76 vol.% of crystals. Earth and Planetary Science Letters, 267(3–4), 571–583. https://doi.org/10.1016/j.epsl.2007.11.065

Crosweller, H. S., Arora, B., Brown, S. K., Cottrell, E., Deligne, N. I., Guerrero, N. O., … Lowndes, J. (2012). Global database on large magnitude explosive volcanic eruptions (LaMEVE). Journal of Applied Volcanology, 1(1), 4.

De Saint Blanquat, M., Horsman, E., Habert, G., Morgan, S., Vanderhaeghe, O., Law, R., & Tikoff, B. (2011). Multiscale magmatic cyclicity, duration of pluton construction, and the paradoxical relationship between tectonism and plutonism in continental arcs. Tectonophysics, 500(1–4), 20–33. https://doi.org/10.1016/j.tecto.2009.12.009

Degruyter, W., & Huber, C. (2014). A model for eruption frequency of upper crustal silicic magma chambers. Earth and Planetary Science Letters, 403, 117–130. https://doi.org/10.1016/j.epsl.2014.06.047

Degruyter, Wim, Huber, C., Bachmann, O., Cooper, K. M., & Kent, A. J. R. (2016). Magma reservoir response to transient recharge events: The case of Santorini volcano (Greece). Geology, 44(1), 23–26. https://doi.org/10.1130/G37333.1

Druitt, T. H., Edwards, L., Mellors, R. M., Pyle, D. M., Sparks, R. S. J., Lanphere, M., … Barreirio, B. (1999). Chapter 3: Development of the Santorini volcanic field in space and time. Geological Society Memoir, 19(1), 13–59. https://doi.org/10.1144/GSL.MEM.1999.019.01.03

Duermeijer, C. E., Nyst, M., Meijer, P. T., Langereis, C. G., & Spakman, W. (2000a). Neogene evolution of the Aegean arc: Paleomagnetic and geodetic evidence for a rapid and young rotation phase. Earth and Planetary Science Letters, 176(3–4), 509–525. https://doi.org/10.1016/S0012-821X(00)00023-6

Duermeijer, C. E., Nyst, M., Meijer, P. T., Langereis, C. G., & Spakman, W. (2000b). Neogene evolution of the Aegean arc: Paleomagnetic and geodetic evidence for a rapid and young rotation phase. Earth and Planetary Science Letters, 176(3–4), 509–525. https://doi.org/10.1016/S0012-821X(00)00023-6

Elburg, M. A., Smet, I., Van den haute, P., Vanhaecke, F., Klaver, M., & Andersen, T. (2018). Extreme isotopic variation documents extensional tectonics in arc magmas from Methana, Greece. Lithos, 318–319, 386–398. https://doi.org/10.1016/j.lithos.2018.08.029

Forni, F., Degruyter, W., Bachmann, O., De Astis, G., & Mollo, S. (2018). Long-Term magmatic evolution reveals the beginning of a new caldera cycle at Campi Flegrei. Science Advances (Vol. 4). https://doi.org/10.1126/sciadv.aat9401

Fowler, S. J., & Spera, F. J. (2010). A metamodel for crustal magmatism: Phase equilibria of giant ignimbrites. Journal of Petrology, 51(9), 1783–1830. https://doi.org/10.1093/petrology/egq039

Fytikas, M., Innocenti, F., Kolios, N., Manetti, P., Mazzuoli, R., Poli, G., … Villari, L. (1986). Volcanology and petrology of volcanic products from the island of Milos and neighbouring islets. Journal of Volcanology and Geothermal Research, 28(3–4), 297–317. https://doi.org/10.1016/0377-0273(86)90028-4

Gottsmann, J., Lavallée, Y., Martí, J., & Aguirre-Díaz, G. (2009). Magma-tectonic interaction and the eruption of silicic batholiths. Earth and Planetary Science Letters, 284(3–4), 426–434. https://doi.org/10.1016/j.epsl.2009.05.008

Gregg, P. M., De Silva, S. L., Grosfils, E. B., & Parmigiani, J. P. (2012). Catastrophic caldera-forming eruptions: Thermomechanics and implications for eruption triggering and maximum caldera dimensions on Earth. Journal of Volcanology and Geothermal Research, 241–242, 1–12. https://doi.org/10.1016/j.jvolgeores.2012.06.009

Hildreth, W., & Lanphere, M. A. (1994). Potassium-argon geochronology of a basalt-andesite-dacite arc system: the Mount Adams volcanic field, Cascade Range of southern Washington. Geological Society of America Bulletin (Vol. 106). https://doi.org/10.1130/0016-7606(1994)106<1413:PAGOAB>2.3.CO;2

Huber, C., Townsend, M., Degruyter, W., & Bachmann, O. (2019). Optimal depth of subvolcanic magma chamber growth controlled by volatiles and crust rheology. Nature Geoscience, 12(9), 762–768. https://doi.org/10.1038/s41561-019-0415-6

Jellinek, A. M., & DePaolo, D. J. (2003). A model for the origin of large silicic magma chambers: Precursors of caldera-forming eruptions. Bulletin of Volcanology, 65(5), 363–381. https://doi.org/10.1007/s00445-003-0277-y

Karlstrom, L., Dufek, J., & Manga, M. (2010). Magma chamber stability in arc and continental crust. Journal of Volcanology and Geothermal Research, 190(3–4), 249–270.

Le Mével, H., Gregg, P. M., & Feigl, K. L. (2016). Magma injection into a long-lived reservoir to explain geodetically measured uplift: Application to the 2007–2014 unrest episode at Laguna del Maule volcanic field, Chile. Journal of Geophysical Research: Solid Earth, 121(8), 6092–6108. https://doi.org/10.1002/2016JB013066

Lejeune, A. M., & Richet, P. (1995). Rheology of crystal-bearing silicate melts: an experimental study at high viscosities. Journal of Geophysical Research, 100(B3), 4215–4229. https://doi.org/10.1029/94JB02985

Malfait, W. J., Seifert, R., Petitgirard, S., Perrillat, J. P., Mezouar, M., Ota, T., … Sanchez-Valle, C. (2014). Supervolcano eruptions driven by melt buoyancy in large silicic magma chambers. Nature Geoscience, 7(2), 122–125. https://doi.org/10.1038/ngeo2042

Meulenkamp, J. E., Wortel, M. J. R., van Wamel, W. A., Spakman, W., & Hoogerduyn Strating, E. (1988). On the Hellenic subduction zone and the geodynamic evolution of Crete since the late Middle Miocene. Tectonophysics, 146(1–4), 203–215. https://doi.org/10.1016/0040-1951(88)90091-1

Nicholls, I. A. (1971). Santorini volcano, greece - tectonic and petrochemical relationships with volcanics of the Aegean region. Tectonophysics, 11(5), 377–385. https://doi.org/10.1016/0040-1951(71)90026-6

Papanikolaou, D., Lekkas, E., Syskakis, D., & Adamopoulou, E. (1993). Correlation on neotectonic structures with the geodynamic activity in Milos during the earthquakes of March 1992. Bulletin of the Geological Society of Greece, 28(3), 413–428.

Papazachos, C. B. (2019). Deep structure and active tectonics of the South Aegean volcanic arc. Elements, 15(3), 153–158. https://doi.org/10.2138/gselements.15.3.153

Parks, M. M., Biggs, J., England, P., Mather, T. A., Nomikou, P., Palamartchouk, K., … Zacharis, V. (2012). Evolution of Santorini Volcano dominated by episodic and rapid fluxes of melt from depth. Nature Geoscience, 5(10), 749–754. https://doi.org/10.1038/ngeo1562

Pe-Piper, G., & Piper, D. J. W. (2005). The South Aegean active volcanic arc: relationships between magmatism and tectonics. Developments in Volcanology, 7(C), 113–133. https://doi.org/10.1016/S1871-644X(05)80034-8

Pe-Piper, Georgia, & Piper, D. J. W. (2007). Neogene backarc volcanism of the Aegean: New insights into the relationship between magmatism and tectonics. Geological Society of America Special Papers, 418(02), 17–31. https://doi.org/10.1130/2007.2418(02)

Pe-Piper, Georgia, & Piper, D. J. W. (2013). The effect of changing regional tectonics on an arc volcano: Methana, Greece. Journal of Volcanology and Geothermal Research, 260, 146–163. https://doi.org/10.1016/j.jvolgeores.2013.05.011

Pe-Piper, Georgia, Piper, D. J. W., & Perissoratis, C. (2005). Neotectonics and the Kos Plateau Tuff eruption of 161 ka, South Aegean arc. Journal of Volcanology and Geothermal Research, 139(3–4), 315–338. https://doi.org/10.1016/j.jvolgeores.2004.08.014

Piper, D. J. W., & Perissoratis, C. (2003). Quaternary neotectonics of the South Aegean arc. Marine Geology, 198(3–4), 259–288. https://doi.org/10.1016/S0025-3227(03)00118-X

Rinaldi, M., & Venuti, M. C. (2003). The submarine eruption of the Bombarda volcano, Milos Island, Cyclades, Greece. Bulletin of Volcanology, 65(4), 282–293. https://doi.org/10.1007/s00445-002-0260-z

Rontogianni, S., Konstantinou, N. S., Melis, C. P., & Evangelidis. (2011). Slab stress field in the Hellenic subduction zone as inferred from intermediate-depth earthquakes. Earth, Planets and Space, 63(2), 139–144. https://doi.org/10.5047/eps.2010.11.011

Singer, B. S., Andersen, N. L., Le Mével, H., Feigl, K. L., DeMets, C., Tikoff, B., … Vazquez, J. (2014). Dynamics of a large, restless, rhyolitic magma system at Laguna del Maule, southern Andes, Chile. GSA Today, 24(12), 4–10. https://doi.org/10.1130/GSATG216A.1

Singer, B. S., Le Mével, H., Licciardi, J. M., Córdova, L., Tikoff, B., Garibaldi, N., … Feigl, K. L. (2018). Geomorphic expression of rapid Holocene silicic magma reservoir growth beneath Laguna del Maule, Chile. Science Advances, 4(6), 1–11. https://doi.org/10.1126/sciadv.aat1513

Smith, V. C., Isaia, R., & Pearce, N. J. G. (2011). Tephrostratigraphy and glass compositions of post-15 ka Campi Flegrei eruptions: Implications for eruption history and chronostratigraphic markers. Quaternary Science Reviews, 30(25–26), 3638–3660. https://doi.org/10.1016/j.quascirev.2011.07.012

Stewart, A. L., & McPhie, J. (2006). Facies architecture and Late Pliocene – Pleistocene evolution of a felsic volcanic island, Milos, Greece. Bulletin of Volcanology, 68(7–8), 703–726. https://doi.org/10.1007/s00445-005-0045-2

Townsend, M., Huber, C., Degruyter, W., & Bachmann, O. (2019). Magma Chamber Growth During Intercaldera Periods: Insights From Thermo−Mechanical Modeling With Applications to Laguna del Maule, Campi Flegrei, Santorini, and Aso. Geochemistry, Geophysics, Geosystems, 20(3), 1574–1591. https://doi.org/10.1029/2018GC008103

Van Hinsbergen, D. J. J., Snel, E., Garstman, S. A., Marunţeanu, M., Langereis, C. G., Wortel, M. J. R., & Meulenkamp, J. E. (2004). Vertical motions in the Aegean volcanic arc: Evidence for rapid subsidence preceding volcanic activity on Milos and Aegina. Marine Geology, 209(1–4), 329–345. https://doi.org/10.1016/j.margeo.2004.06.006

Voight, B., Sparks, R. S. J., Miller, A. D., Stewart, R. C., Hoblitt, R. P., Clarke, A., … Young, S. R. (1999). Magma flow instability and cyclic activity at Soufriere Hills volcano, Montserrat, British West Indies. Science, 283(5405), 1138–1142. https://doi.org/10.1126/science.283.5405.1138

Walcott, C. R., & White, S. H. (1998). Constraints on the kinematics of post-orogenic extension imposed by stretching lineations in the Aegean region. Tectonophysics, 298(1–3), 155–175. https://doi.org/10.1016/S0040-1951(98)00182-6

White, S. M., Crisp, J. A., & Spera, F. J. (2006). Long-term volumetric eruption rates and magma budgets. Geochemistry, Geophysics, Geosystems, 7(3), 262–266. https://doi.org/10.1029/2005GC001002

Wijbrans, J., Németh, K., Martin, U., & Balogh, K. (2007). 40Ar/39Ar geochronology of Neogene phreatomagmatic volcanism in the western Pannonian Basin, Hungary. Journal of Volcanology and Geothermal Research, 164(4), 193–204. https://doi.org/10.1016/j.jvolgeores.2007.05.009

Zhou, X., Kuiper, K., Wijbrans, J., Boehm, K., & Vroon, P. (2020). Eruptive history and 40Ar/39Ar geochronology of the Milos volcanic field, Greece. Geochronology Discussions, 2020, 1–40. https://doi.org/10.5194/gchron-2020-30